Preprint Title	Polymeric Ionomer-Mediated Electrodeposition of $Mn(OH)_2$ Nanonets on Carbon Nanofibers toward Enhanced Electrochemical Performance
Authors	Yeji Yim, Myung Hwa Kim and Dasol Jin
Publication Date	29 Jan. 2026
Article Type	Full Research Paper
Supporting Information File 1	SI_Mn(OH)x-Dep.docx; 928.9 KB
ORCID® iDs	Yeji Yim - https://orcid.org/0009-0001-5770-8793; Myung Hwa Kim - https://orcid.org/0000-0001-7254-2886

Polymeric Ionomer-Mediated Electrodeposition of $Mn(OH)_2$ Nanonets on Carbon Nanofibers toward Enhanced Electrochemical Performance

Yeji Yim[1], Myung Hwa Kim[1,2,*] and Dasol Jin[3,*]

Address: [1]Department of Chemistry and Nanoscience, Ewha Womans University, Seoul 03760, Republic of Korea

[2]Institute of Multiscale Matter and System (IMMS), Ewha Womans University, Seoul 03760, Republic of Korea

[3]Department of Chemistry, Jeonbuk National University, Jeonju 54896, Republic of Korea

Email: Dasol Jin (dasoljin@jbnu.ac.kr) and Myung Hwa Kim (myungkim@ewha.ac.kr)

* Corresponding author

Abstract

Engineering metal hydroxide–carbon interfaces with controlled microstructure is critical for optimizing electrochemical performance, yet conventional fabrication strategies often suffer from non-uniform deposition and weak interfacial coupling. Herein, we report an electrodeposition-driven strategy to construct $Mn(OH)_2$-decorated carbon nanofiber (CNF) electrodes with tunable morphology and enhanced electrochemical activity. Importantly, polymeric ionomer (Nafion) is employed as a microenvironment-regulating medium, functioning as a binder to govern $Mn(OH)_2$ growth. Specifically,

systematic modulation of Nafion concentration induces distinct $Mn(OH)_2$ deposition morphologies, which in turn give rise to pronounced differences in electrical conductivity and interfacial charge-transfer kinetics. The optimized $Mn(OH)_2$/CNF electrodes exhibit the enhanced oxygen evolution reaction activity with lowered charge-transfer resistance, demonstrating the strong correlation between deposition microenvironment, morphological evolution, and electrochemical performance.

Keywords

carbon nanofiber; polymeric ionomer; electrodeposition; manganese hydroxide; oxygen evolution reaction

Introduction

Electrochemical performance of carbon-based electrodes can be significantly enhanced through surface functionalization with transition-metal hydroxides or oxides, which introduce additional redox-active sites and improve interfacial charge-transfer kinetics as well as intrinsic electrical conductivity [1-3]. Among various strategies, integrating metal precursors onto conductive carbon substrates has attracted increasing attention [4,5], as it enables synergistic coupling between the high electrical conductivity of carbon frameworks and the catalytic or pseudocapacitive properties of metal species. However, conventional approaches such as hydrothermal growth, impregnation–calcination or physical mixing often suffer from limited interfacial contact, non-uniform metal distribution and poor controllability over surface chemistry, ultimately restricting electrochemical efficiency [6-8]. To overcome these limitations, electrodeposition has emerged as a powerful technique for metal precursor integration, offering precise control over deposition potential, duration and precursor concentration.

This electrochemical approach enables preferential nucleation of metal precursors at electroactive sites of carbon nanofibers, forming conformal coatings or nanoscale clusters without the need for high-temperature treatment [9,10].

Compared with other template-free approaches such as chemical vapor deposition, thermal vapor transport and laser-assisted growth, electrochemical deposition on carbon substrates provides a versatile route for constructing hierarchical architectures by directly modifying morphologically controlled conductive frameworks [11,12], thereby enabling immediate applicability across diverse electrochemical systems. In this context, manganese-based precursors are particularly attractive owing to their earth abundance, low toxicity, and rich multivalent redox chemistry, which enables reversible $Mn^{2+}/Mn^{3+}/Mn^{4+}$ transitions and provides abundant pseudocapacitive sites for electrochemical energy storage and catalytic applications [13-15]. Moreover, manganese hydroxide species exhibit strong affinity toward hydroxylated carbon surfaces and favorable proton-coupled electron-transfer behavior, making them highly suitable for electrochemical environments [16]. These attributes render manganese precursors a chemically versatile platform for tailoring interfacial charge storage and reaction pathways while maintaining material sustainability and cost effectiveness.

Herein, we demonstrate an electrodeposition-driven strategy to decorate carbon nanofibers with $Mn(OH)_2$, yielding structurally integrated hybrid electrodes with enhanced electrochemical performance. By integrating metal precursor electrodeposition with Nafion-mediated microenvironmental control, Nafion functions beyond its conventional role as a binder and instead acts as an active regulating medium that governs $Mn(OH)_2$ growth behavior. Varying Nafion concentration leads to distinct $Mn(OH)_2$-deposition morphologies, which in turn translate into pronounced

differences in electrical conductivity and charge-transfer kinetics, manifested by improved oxygen evolution reaction activity.

Results and Discussion

Figure 1 illustrates the overall preparation process of $Mn(OH)_2$-decorated carbon nanofiber electrodes. Carbon nanofibers (CNFs) as the conductive framework were first fabricated by electrospinning and subsequent thermal treatment via carbonization. Nafion was then introduced onto the as-prepared CNFs to tailor the local deposition microenvironment, followed by electrochemical deposition of $Mn(OH)_2$. During electrodeposition, Mn^{2+} ions undergo localized hydrolysis near the cathodic surface [17], leading to the formation of $Mn(OH)_2$ directly on CNFs. Importantly, Nafion plays a dual role as both a proton-regulating medium and an ion-conducting binder [18], enabling controlled nucleation and growth of $Mn(OH)_2$ through modulation of local ionic transport.

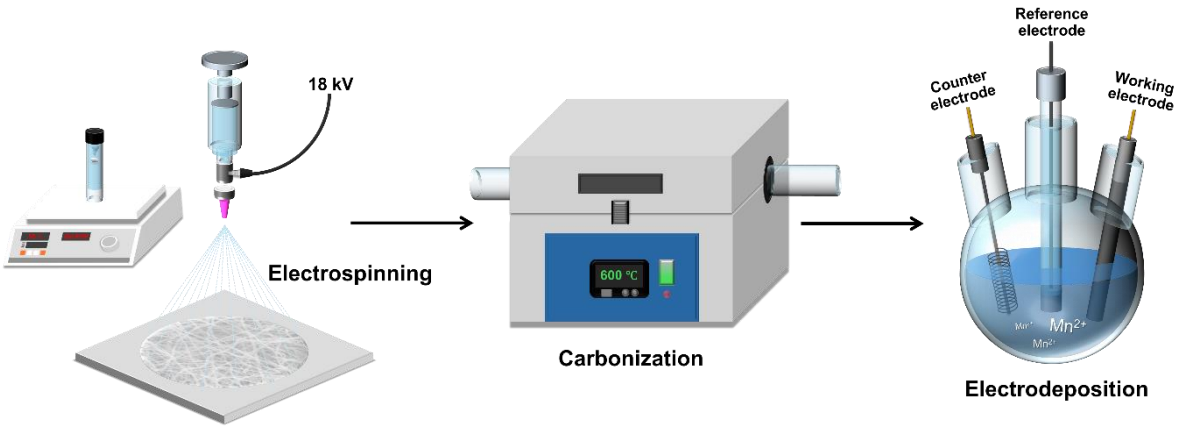

Figure 1: Schematic illustration of synthesis of $Mn(OH)_2$-decorated carbon nanofiber electrodes.

Electrodeposition was carried out by cyclic voltammetry over a potential range of 0.6-1.2 V for 10 cycles in an aqueous electrolyte containing 1.0 mM $Mn(CH_3COO)_2$

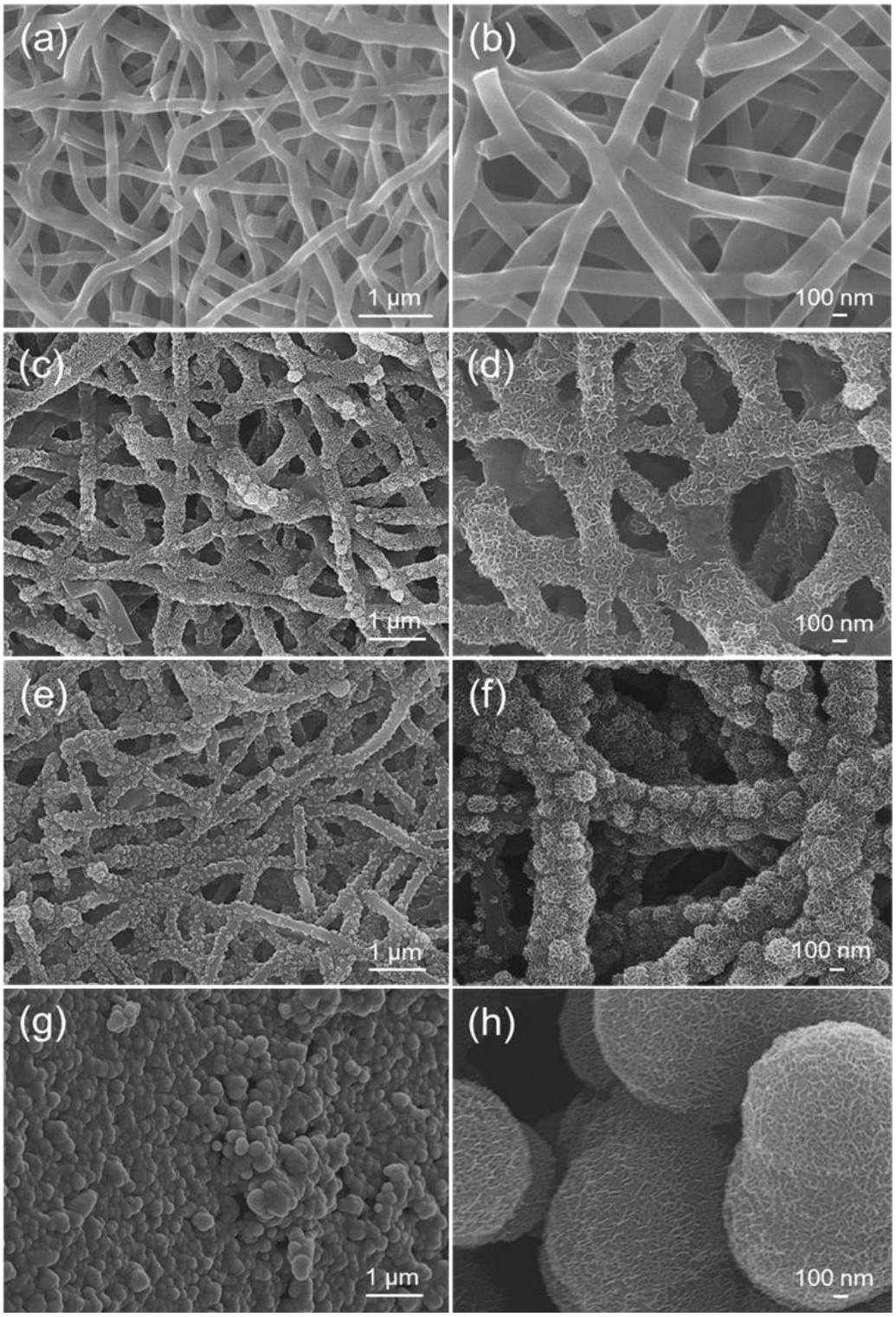

Figure 2: FE-SEM images of $Mn(OH)_2$ electrodeposited on carbon nanofibers with different Nafion coating concentrations: (a,b) pristine carbon nanofiber, (c,d) 0.2 wt%, (e,f) 0.5 wt%, and (g,h) 1.0 wt%.

(Figure S1). Subsequently, the as-prepared electrodes showed distinct morphological features, as shown in SEM images (Figure 2). In contrast to pristine CNFs with smooth surfaces (Figures 2a and 2b), $Mn(OH)_2$ is sparsely distributed at a low Nafion concentration (0.2 wt%), indicating insufficient nucleation on the substrates (Figures 2c and 2d). Note, as shown in Figure S2, $Mn(OH)_2$ electrodeposition is negligible on pristine CNFs in the absence of Nafion coating, underscoring the critical role of Nafion in facilitating nucleation and growth. At an intermediate Nafion concentration (0.5 wt%; Figures 2e and 2f), uniform nanoscale $Mn(OH)_2$ decoration is achieved along individual nanofibers, underscoring the advantage of the three-dimensional CNF network in promoting homogeneous nucleation and enhanced interfacial contact. In contrast, at a high Nafion concentration (1.0 wt%; Figures 2g and 2h), aggregated $Mn(OH)_2$ domains are observed, accompanied by excessive deposition across the entire substrate, which ultimately obscures the intrinsic CNF morphology.

These structural distinctions establish CNFs as an ideal platform for electrodeposition-driven surface functionalization. XPS was employed to elucidate the chemical states of $Mn(OH)_2$ deposited on CNFs as a function of Nafion concentration. In O 1s region (Figure 3a), all samples exhibit two characteristic components centered at ~532 and ~529 eV, which are assigned to Mn–OH and Mn–O–Mn species,

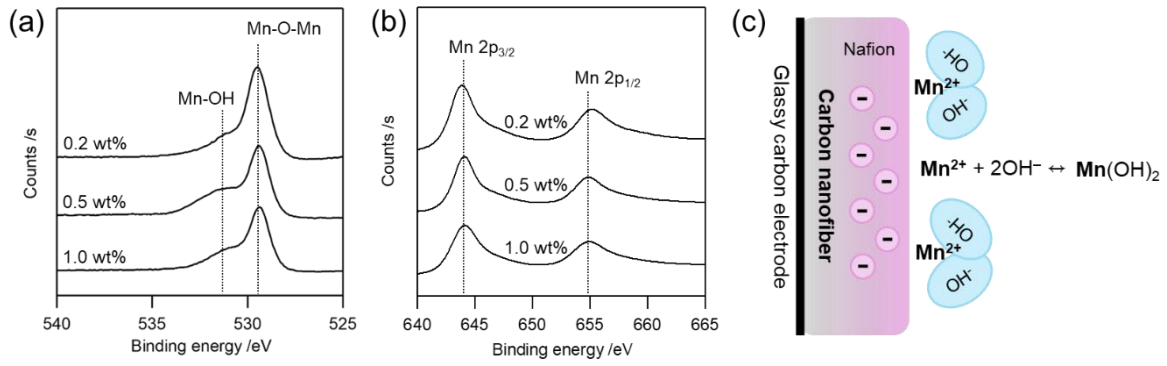

Figure 3: XPS spectra of as-prepared electrodes with different Nafion concentrations in (a) O 1s and (b) Mn 2p regions, and (c) schematic illustration of Nafion–dependent electrodeposition mechanism.

respectively, confirming the presence of hydroxylated manganese oxide environments [19]. Figure 3(b) presents the spectra in Mn 2p region, where two prominent peaks at approximately 644 and 654 eV correspond to Mn $2p_{3/2}$ and Mn $2p_{1/2}$, indicative of Mn^{2+} species [20]. Collectively, these XPS results verify the successful formation of $Mn(OH)_2$ across all three $Mn(OH)_2$-decorated CNF electrodes prepared under different Nafion concentrations. More importantly, Figure 3(c) schematically illustrates the electrodeposition mechanism proposed in this study. The Nafion coating, bearing

negatively charged sulfonate groups, facilitates local proton retention and Mn^{2+} transport, thereby promoting the nucleation and growth of $Mn(OH)_2$ across the CNF surface [21]. Consequently, the $Mn(OH)_2$ deposition behavior exhibits a strong dependence on Nafion concentration. At low Nafion content, insufficient proton regulation and weak ionic pathways lead to sparse $Mn(OH)_2$ nucleation, resulting in isolated deposits. In contrast, excessive Nafion forms a thick polymeric layer that partially impedes electron transfer and mass transport, thereby suppressing effective $Mn(OH)_2$ deposition.

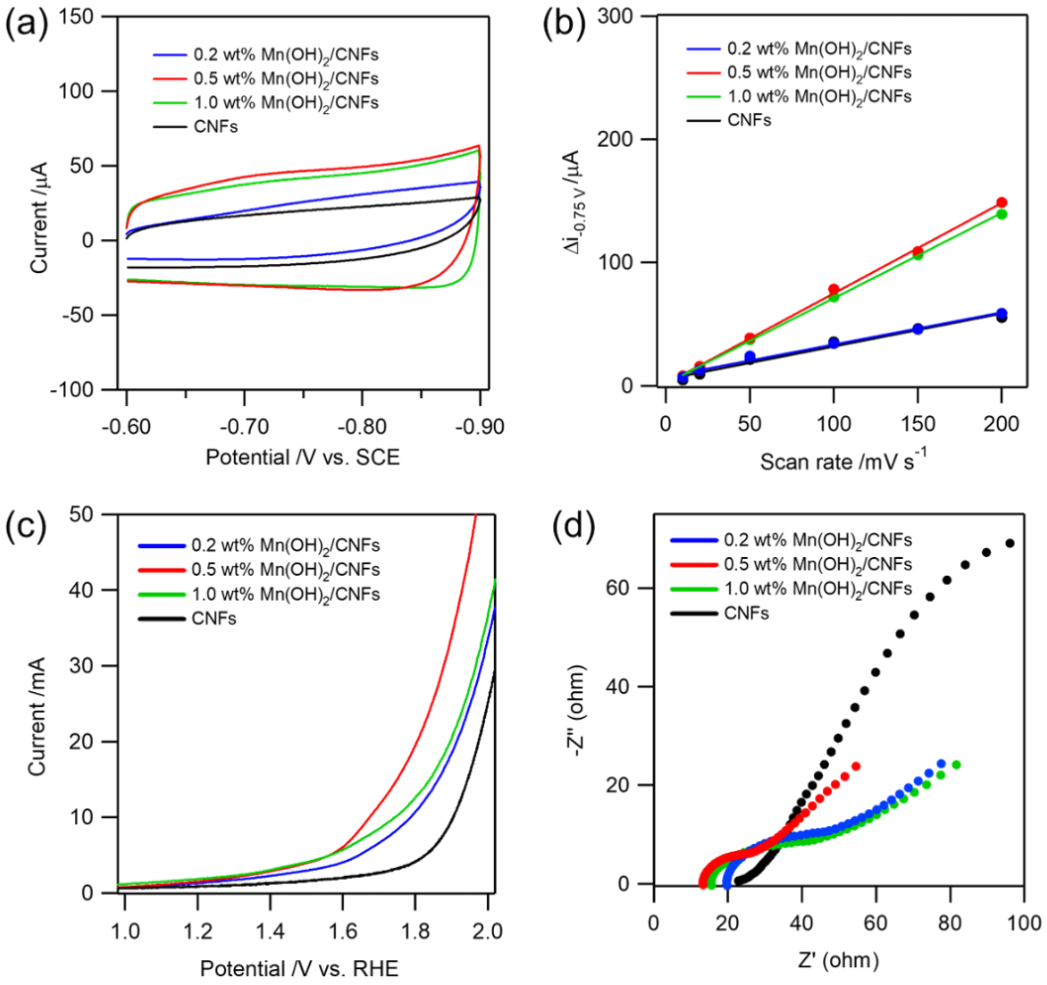

Figure 4: Electrochemical performance of $Mn(OH)_2$/CNF electrodes prepared with different Nafion concentrations: (a) overlaid cyclic voltammograms recorded at 100 mV s^{-1} in 1.0 M KNO_3, (b) plots of the absolute charging/discharging current differences at –0.75 V ($\Delta i_{-0.75\ V}$) *vs*. scan rate, (c) LSV curves, and (b) Nyquist plots. The cyclic voltammograms corresponding to (a) and (b) are provided in Figure S3.

The electrochemical properties of Nafion-regulated $Mn(OH)_2$ deposition on CNFs (denoted as *x* wt% $Mn(OH)_2$/CNFs, where *x* represents the Nafion concentration used during synthesis) were evaluated. To examine the interfacial capacitive behavior of the $Mn(OH)_2$/CNF electrodes prepared with different Nafion concentrations, cyclic voltammograms were recorded in the non-faradaic potential region at scan rates ranging from 10 to 200 mV s^{-1} (Figure S3). As shown by the overlaid CVs collected at 100 mV s^{-1} in Figure 4(a), Nafion-coated CNFs exhibit enhanced current responses compared to bare CNFs. For all samples, the current response increases linearly with scan rate, indicating dominant capacitive behavior [22]. Notably, the 0.5 wt% $Mn(OH)_2$/CNF electrode fabricated with an intermediate Nafion concentration displays a significantly larger enclosed CV area than those prepared with either lower or higher Nafion contents, suggesting an increased density of electrochemically accessible surface sites. As shown in Figure 4(b), plotting the absolute difference between anodic and cathodic current densities (Δi) at –0.75 V as a function of scan rate yields linear fits for all samples (R^2 = 0.9992). Notably, the $Mn(OH)_2$/CNF electrode prepared with 0.5 wt% Nafion exhibits the highest slopes, confirming the presence of a larger electrochemically active interface. This enhancement can be attributed to ionomer-mediated regulation of $Mn(OH)_2$ nucleation and growth, which promotes the formation of interconnected nanonet structures with increased surface exposure and improved electrolyte accessibility.

Consistent with this behavior, the electrodes prepared with the optimized Nafion concentration display markedly enhanced electrochemical oxygen evolution reaction relative to both bare CNFs and the electrodes fabricated with suboptimal Nafion contents, as shown in Figure 4(c). Specifically, the optimized electrode delivers higher current density and a lower onset potential in LSV measurements. Furthermore, EIS analysis (Figure 4d) reveals a reduced charge-transfer resistance for the optimized

$Mn(OH)_2$/CNF electrode, confirming improved interfacial conductivity and accelerated electron-transport pathways [23]. This enhanced performance arises from the synergistic integration of $Mn(OH)_2$ and CNFs under a Nafion-regulated deposition environment, where appropriate Nafion content optimizes ionic accessibility without impeding charge transfer. These results demonstrate that Nafion-mediated electrodeposition provides an effective strategy for engineering metal hydroxide–carbon interfaces with tunable morphology and enhanced electrochemical functionality.

Conclusion

In summary, we demonstrate a Nafion-mediated electrodeposition strategy for fabricating $Mn(OH)_2$-decorated carbon nanofiber (CNF) electrodes with tunable morphology and enhanced electrochemical performance. By directly integrating $Mn(OH)_2$ onto conductive CNF substrates, homogeneous nanoscale decoration is achieved without the need for multistep synthesis or post-thermal treatment. Importantly, Nafion concentration is identified as a key parameter governing the local electrodeposition microenvironment, regulating ionic accessibility and $Mn(OH)_2$ nucleation behavior. The optimized $Mn(OH)_2$/CNF electrodes exhibit accelerated charge-transfer kinetics and reduced interfacial resistance, leading to markedly improved electrochemical activity. This work, therefore, reports electrodeposition-assisted microenvironment engineering as an effective approach for constructing metal hydroxide–carbon hybrid electrodes and offers a scalable platform for designing advanced electrochemical interfaces for energy conversion and storage applications.

Experimental

Materials: Polyacrylonitrile (PAN), N,N-dimethylformamide (DMF), manganese(II) acetate ($Mn(CH_3CO_2)_2$) and Nafion were purchased from Sigma-Aldrich (St. Louis, MO, USA). Ethanol (EtOH, 99.9%) was purchased from Daejung (Korea). All aqueous solutions were prepared using deionized water (resistivity ≥ 18 MΩ·cm). All chemicals were of analytical grade and used without further purification.

Fabrication of Carbon Nanofibers: Carbon nanofibers (CNFs) were prepared by electrospinning followed by thermal treatment. PAN (300 mg) was dissolved in DMF (1.6 mL) to obtain a homogeneous spinning solution. Electrospinning was conducted at an applied voltage of 18 kV with a feeding rate of 1.2 mL h^{-1} and a tip-to-collector distance of 15 cm. The collected PAN nanofibers stabilized in air at 180 °C for 1 h and subsequently carbonized under Ar atmosphere at 600 °C for 3 h. The resulting CNFs were used as conductive substrates.

Electrodeposition: CNF electrodes were prepared using Nafion solutions with different concentrations. Nafion stock solution (5 wt%) was diluted with ethanol to obtain Nafion concentrations of 0.2, 0.5 and 1.0 wt%. The CNF substrates were coated with Nafion by drop-casting 10 µL of solution and dried at room temperature. $Mn(OH)_2$ was electrodeposited in a three-electrode configuration using 45 µg-loaded CNF onto GC electrode (d = 3 mm) as the working electrode, Pt wire as the counter electrode, and saturated calomel electrode (SCE) as the reference electrode. Electrodeposition was performed by repetitive cyclic voltammetry between 0.6 and 1.2 V for 10 cycles in an aqueous electrolyte containing 1.0 mM $Mn(CH_3COO)_2$. After deposition, the electrodes were rinsed with DI water and dried.

Physical Characterization: The morphology characterization was examined using field-emission scanning electron microscopy (FE-SEM; JEOL JSM-6700F). Surface

chemical states and crystallographic structures were analyzed by angle-resolved X-ray photoelectron spectroscopy (AR-XPS; Thermo Fisher Scientific K-ALPHA XPS, Al Kα radiation at 12 kV).

Electrochemical Characterization: All electrochemical measurements were performed in a standard three-electrode configuration, employing the as-prepared $Mn(OH)_2$/CNFs as the working electrode, a SCE as the reference electrode, and a coiled Pt wire as the counter electrode. The OER activity was evaluated by rotating disk electrode (RDE) voltammetry using an electrochemical analyzer (RDE-1 rotor/Epsilon electrochemical analyzer, BASi) in N_2-saturated 1 M KOH (*aq*) at a rotation rate of 1600 rpm. Current densities were calculated by normalizing the measured current to the geometric surface area (GSA) of the electrode. The GSAs were determined by chronocoulometry measurements in 0.1 M KNO_3 containing 10 mM $K_3Fe(CN)_6$ [24]. All electrochemical measurements were performed using a CHI 920C electrochemical workstation (CH Instruments). AC electrochemical impedance spectroscopy (EIS) measurements were conducted in 1 M KOH (*aq*) at potentials corresponding to an OER current density of 10 mA cm^{-2} for each electrocatalyst, over a frequency range from 1 Hz to 10 kHz. The *i*R drop in the three-electrode configuration was automatically compensated.

Supporting Information

Supporting Information File 1:

File Name: SI_Mn(OH)x-Dep

File Format: docx

Title: Polymeric Ionomer-Mediated Electrodeposition of $Mn(OH)_2$ Nanonets on Carbon Nanofibers toward Enhanced Electrochemical Performance

Acknowledgement

The authors declare that they have no known competing financial interests or personal relationships that could have appeared to influence the work reported in this paper. D.J. gratefully acknowledge support from Department of Chemistry, College of Natural Science at Jeonbuk National University.

Funding

This work was financially supported by the National Research Foundation of Korea (NRF) funded by the Ministry of Science and ICT or by the Ministry of Education (NRF-RS-2018-NR031064 and RS-2025-16063688).

References

1. Kothandam, G.; Singh, G.; Guan, X.; Lee, J. M.; Ramadass, K.; Joseph, S.; Benzigar, M.; Karakoti, A.; Yi, J.; Kumar, P.; Vinu, A. *Adv. Sci.* **2023**, *10*, 2301045.
2. Karamveer, S.; Thakur, V. K.; Siwal, S. S. *Mater. Today.: Proc.* **2022**, *56*, 9-17
3. Zhu, J.; Lu, X. F.; Luan, D.; Lou, X. W. *Angew. Chem. Int. Ed.* **2024**, *63*, e202408846.
4. Xu, C.; Li, Y.; Li, D.; Zhang, Y.; Liu, B.; Hasan Akhonb, M. D.; Huo, P. *Nanoscale*, **2024**, *16*, 8286-8306.
5. Hammel, E.; Tang, X.; Trampert, M.; Schmitt, T.; Mauthner, K.; Eder, A.; Pötschke, P. *Carbon*, **2004**, *42* (5–6), 1153–1158.
6. Wang, T.; Chen, Z.; Gong, W.; Xu, F.; Song, X.; He, X.; Fan, M. *ACS Omega* **2023**, *8* (25), 22316–22330.

7. Kim, M.; Lee, S.; An, Z.; Joo, H.; Cho, J.; Baek, J.; Hwang, U.; Yang, X.; Qin, J.; Kwon, J.; Yang, K.; Kim, S.; Park, S. *Carbon Neutralization* **2026**, *5* (1), e70108.
8. Zhang, X.; Li, X.; Zhang, X.; Yu, H.; Sun, R.; Ge, C.; Yang, X.; Liu, Y.; Fang, J. *Small* **2025**, *21* (43), e04846.
9. Ping, Z.; Junjie, L.; Yunchun, L. *RSC Adv.* **2022**, *12*, 18134-18143.
10. Huang, S.; Bi, D.; Xia, Y.; Lin, H. *ACS Appl. Energy Mater.* **2023**, *6* (2), 856–864.
11. Dammu, S.; Singh, A. P.; Lala, S. R. F.; Srivastava, C. *Metall Mater Trans A* **2023**, *54*, 3928–3939.
12. Hannula, P.-M.; Peltonen, A.; Aromaa, J.; Janas, D.; Lundström, M.; Wilson, P. B.; Koziol, K.; Forsén, O. *Carbon*, **2016**, *107*, 381–387.
13. Samuel, E.; Joshi, B.; Huh, J.; Kim, S.; Park, M.; Lee, H.-S.; Yoon, S. S. *Appl. Surf. Sci.* **2026**, *718*, 164884.
14. Kim, S. E.; Yoon, J. C.; Tae, H.-J.; Muthurasu, A. *ACS Omega* **2023**, *8* (45), 42689–42698.
15. Si, P.; Chena, P.; Kim, D.-H. *J. Mater. Chem. B* **2013**, *1*, 2696-2700.
16. Qu, X. *Sustainable Energy res.* **2025**, *12*, 67.
17. Sambandam, B.; Mathew, V.; Kim, S; Lee, S.; Kim, S.; Hwang, J. Y.; Fan, H. J.; Kim, J. *Chem* **2022**, *8* (4), 924–946.
18. He, S.; Chai, S.; Li, H. *ChemSusChem* **2025**, *18*, e202402506.
19. Xu, G.-R.; Xie, C.-P.; Wen, Y.; Tang, A.-P.; Song, H.-S. *Ionics* **2019**, *25*, 3287–3298.
20. Yang, Z.; Gong, J.; Tang, C.; Zhu, W.; Cheng, Z.; Jiang, J.; Ma, A.; Ding, Q. *J. Mater. Sci.: Mater. Electron.* **2017**, *28*, 17533–17540.
21. Mayadevi, T. S.; Goo, B.-H.; Paek, S. Y.; Choi, O.; Kim, Y.; Kwon, O. J.; Lee, S. Y.; Kim, H.-J.; Kim, T.-H. *ACS Omega* **2022**, *7* (15), 12956–12970.
22. Frackowiak, E.; Béguin, F. *Carbon* **2001**, *39*, 937–950.

23. An, H.; Park, W.; Shin, H.; Chung, D. Y. *EcoMat.* **2024**, *6* (10), e12486.

24. Jin, D.; Woo, H.; Prabhakaran, S.; Lee, Y.; Kim, M. H.; Kim, D. H.; Lee, C. *Adv. Funct. Mater.* **2023**, *33*, 2301559.